Oral butyrate reduces progression of kidney damage in an L-NAME-Induced diabetic kidney disease mouse model

Nicese, M.N.; Koudijs, A.; Lalai, R.; Avramut, C.; Derks, R.J.E.; Sánchez-López, E.; ... ; Rotmans, J.I.

Diabetes, Obesity and Metabolism

WILEY

ORIGINAL ARTICLE OPEN ACCESS

Oral Butyrate Reduces Progression of Kidney Damage in an L-NAME-Induced Diabetic Kidney Disease Mouse Model

Maria Novella Nicese[1,2] | Angela Koudijs[1,2] | Reshma Lalai[1,2,3] | Cristina Avramut[4] | Rico J. E. Derks[5] | Elena Sánchez-López[5] | Martin Giera[5] | Amanda C. M. Pronk[2,3] | Artemiy Kovynev[2,3] | Sander Kooijman[2,3] | Patrick C. N. Rensen[2,3] | Roel Bijkerk[1,2] | Bernard M. van den Berg[1,2] | Joris I. Rotmans[1,2]

[1]Department of Internal Medicine, Division of Nephrology, Leiden University Medical Center, Leiden, the Netherlands | [2]Einthoven Laboratory for Experimental Vascular Medicine, Leiden University Medical Center, Leiden, the Netherlands | [3]Department of Internal Medicine, Division of Endocrinology, Leiden University Medical Center, Leiden, the Netherlands | [4]Department of Cell and Chemical Biology, Leiden University Medical Center, Leiden, the Netherlands | [5]Center for Proteomics and Metabolomics, Leiden University Medical Center, Leiden, the Netherlands

Correspondence: Maria Novella Nicese (m.n.nicese@lumc.nl) | Joris I. Rotmans (j.i.rotmans@lumc.nl)

Received: 17 March 2026 | **Revised:** 6 August 2026 | **Accepted:** 7 August 2026

Handling Editor: Nigel Irwin

Keywords: cardiovascular disease | diabetic nephropathy | dietary intervention | type 2 diabetes

ABSTRACT

Aims: Diabetic kidney disease (DKD) is one of the main causes of kidney failure worldwide. Interestingly, patients affected by DKD are characterised by a low abundance of gut bacteria producing short fatty acids including butyrate, which is suggested to play a role in the decline of renal function. Consequently, we aimed to test the effects of oral butyrate supplementation on kidney health in mice affected by DKD.

Material and Methods: To this end, we treated diabetic BKS *db/db* mice (C57BLKS/J *Lepr*^{db}) via drinking water with the eNOS inhibitor N(ω)-nitro-L-arginine methyl ester (L-NAME), which accelerates the progression of DKD. Simultaneously, mice were fed low-fat chow with or without 5% butyrate.

Results: Oral butyrate supplementation reduced mesangial expansion, glomerular enlargement and medullary fibrosis in kidney biopsies of the mice. These protective effects correlated with an increased abundance of *Akkermansiaceae* in the gut. In mice treated with butyrate, the abundance of *Akkermansiaceae* positively correlated with glomerular filtration rate (GFR) and plasma concentration of indole-3-methyl acetate and indole-3-acetaldehyde, key metabolites associated with many beneficial cardiovascular effects.

Conclusions: In conclusion, oral butyrate supplementation in mice with DKD improves kidney morphology, accompanied by an increased abundance of *Akkermansiaceae* in the gut. Future studies, such as transplantation of *Akkermansia*, should reveal whether this relationship is causal and translate into improved kidney function in DKD.

1 | Introduction

Diabetic kidney disease (DKD) represents one of the most frequent and severe complications of diabetes and a major cause of end stage kidney disease globally [1–3]. DKD is a complex disease caused by the concurrence of multiple factors, including hyperglycemia, hypertension and inflammation [4–6]. Moreover, diabetes mellitus (DM) can drastically alter the composition of the intestine, which is increasingly emerging as key determinant for DKD progression. Numerous studies have shown the correlation between DKD and gut microbiome composition, which is different and less diverse in DKD patients when compared to healthy subjects [7–11]. Specifically, patients affected by DM and chronic kidney disease (CKD) tend to show a reduction

in bacteria producing short chain fatty acids (SCFAs), such as butyrate, acetate and propionate [12–14]. These metabolites are typically linked to beneficial effects such as the promotion of intestinal integrity and the regulation of immune responses [15–19]. Amongst SCFAs, butyrate is most extensively studied, as it can regulate gene expression and cellular signalling, besides playing a crucial role in mitochondrial homeostasis and cellular metabolism [20, 21].

Butyrate has been shown to prevent the expression of pro-inflammatory and pro-fibrotic markers in renal tubular epithelial cells and podocytes [22], while it improves mitochondrial function and boosts the expression of tight junction proteins in glomerular endothelial cells [23–25]. Multiple studies have also shown that butyrate can mitigate DM by increasing insulin sensitivity [26, 27] and reducing appetite as well as food intake and fat mass in mice fed a high-fat diet [28]. Similar effects were also reported in *db/db* mice, where butyrate supplementation in combination with either SGLT2 inhibitors [29] or metformin [23] further reduces body weight, blood glucose and blood urea nitrogen (BUN). Interestingly, Tang et al. demonstrated that, in addition to differences in gut microbiome composition, patients with DKD have a lower plasma concentration of butyrate compared to healthy subjects [30]. This confirms that the circulating levels of this metabolite negatively correlate with DKD progression.

In this study, we aimed to investigate whether oral butyrate supplementation can prevent kidney injury and slow down the decline in kidney function in diabetic mice. To address this hypothesis, we supplemented butyrate orally to a mouse model of DKD that is accelerated by administering the eNOS inhibitor N(ω)-nitro-L-arginine methyl ester (L-NAME) to BKS db/db mice, which develop hyperglycemia and obesity [31].

2 | Material and Methods

2.1 | Animals

This study was performed in compliance with Dutch government guidelines, the Directive 2010/63/EU of the European Parliament and was approved by the Institutional Committee for Animal Welfare at the Leiden University Medical Center.

Eight-week-old male BKS.Cg-*Dock7*^{m} +/+ *Lepr*^{db}/J mice (JAX Mice Strain) were purchased from Charles River Laboratories (Den Bosch, the Netherlands). Mice were housed in pairs with a light–dark cycle of 12 h each, with unrestricted access to water and regular chow, containing 10 kJ% fat, 20 kJ% protein and 70 kJ% carbohydrates (Ssniff, Soest, Germany). After 1 week of acclimation and baseline measurements, mice were randomly assigned to two groups ($n = 10$ per group): one control group that received L-NAME via drinking water and an intervention group, that was given L-NAME via drinking water and chow enriched with 5% sodium butyrate. The 5% dietary supplementation of sodium butyrate has been chosen based on previous literature commonly reported in chronic murine studies [28, 32–34]. Approximately 80 mg/kg/day of L-NAME (N5751, Sigma, Saint Louis, MO) was administered, for which the concentration in the drinking water was adjusted according to the average mouse weight and water intake per cage and replaced twice a week for 4 weeks. After 4 weeks from the start of the intervention, animals were euthanised and organs collected.

2.2 | Glomerular Filtration Rate (GFR) Measurements

GFR measurements were performed using the transdermal mini GFR from MediBeacon (Creve Coeur, MO) [35]. To measure GFR, mice were first anaesthetised with isoflurane and then shaved on one of the flanks while being on a heating pad. Afterwards, the GFR measuring device was connected to the battery and then applied on the skin of the animal with the help of extra tape in order to secure it. When the animals were still under anaesthesia, a solution of FITC-sinistrin (FTC-FS001, MediBeacon) was injected through tail vein at a concentration of 0.15 mg/g of body weight. Once the FITC-sinistrin had been injected, the mice were single-housed in an empty cage without food, water, or enrichment. After 1 h, the device was removed and the data collected.

2.3 | Mean Arterial Blood Pressure (MABP) and Pulse Measurements

MABP and pulse were measured through the tail-cuff technique by using the BP-2000 Blood Pressure Analysis System machine from Visitech Systems (United States, Napa, NC). Before starting with the measurements, animals were located on the heating platform (36°C) of the machine and immobilised with the proper restrainer, before putting the cuff around their tail. After 5 min, the acclimatisation measurements started, followed by the actual measurements.

2.4 | Urine Collection

Urine was collected by using the hydrophobic sand from LabSand (LABSAND CS, BiosebLab, Vitrolles, France). After dividing the sand equally in clean empty small cages, animals were housed separately until urine was produced and immediately collected. Afterwards, animals were returned to their own cage, together with their littermates.

2.5 | Blood Glucose Measurements

To measure blood glucose level, we used the glucometer Accu-Chek Performa together with Accu-Chek Performa strips (650 159, La Roche, Basel, Switzerland). After puncturing the tail of the mice, a drop of blood was used to measure glucose.

2.6 | Urinary Albumin-To-Creatinine Ratio

Albumin and creatinine in urine were measured by using Mouse albumin ELISA kit (ab108792, Abcam, Cambridge, Great Britain) and Mouse creatinine assay kit (80 350, Bio-Connect, Huissen, the Netherlands), respectively, according to manufacturers' instructions.

2.7 | Body Composition and Body Water Content

Body composition and body water content were measured in conscious mice using an EchoMRI-100 Analyser (EchoMRI, Houston, Texas).

2.8 | Histological Analysis

After perfusing the arterial circulation of the animals with a pump (pressure 150 mmHg) via the heart with a solution of ice-cold PBS and 0.5 IU/mL of heparin (B01AB01—Heparin), kidneys were vertically cut and two half kidneys were fixed in a solution of 4% formaldehyde (ROL.1642810, Added Pharma, Oss, the Netherlands) and then embedded in paraffin.

To study kidney morphology, 4-μm thick paraffin sections were stained with period acid-Schiff solution (3 952 016, Sigma Aldrich) or direct red (365 548, Sigma Aldrich)–fast green solution (F7258), resulting in PAS staining or Sirius red staining, respectively.

To assess collagen I deposition in kidney tissue, paraffin sections were treated with citrate buffer for antigen retrieval. Next, permeabilisation was performed with a solution of 0.1% Tween (8.22184.0500, Merck, Darmstadt, Germany) in PBS, followed by a blocking step with a solution of 5% bovine serum albumin (BSA) (A7906, Sigma Aldrich) also in PBS. Tissue slides were then incubated with the primary antibody against collagen I (Ab21286, Abcam) overnight at 4°C. The next day, slides were incubated with secondary antibody (HRP antibody, P0450, DAKO, Denmark) for 1 h. Afterwards a solution of tyramide FITC (46 410, Thermo Fisher, Waltham, MS) was added, followed by DAB (DAKO, K3468) staining to visualise the reaction. Eventually a counterstaining was performed with Mayer's hemalum solution (Merck, 1.09249) before the final washing steps and mounting.

To visualise vessels, antibodies against MECA32 (BioLegend, 120 501) and CD31 (Dianova, DIA-310) were utilised to stain kidney sections. After overnight incubation with primary antibodies, slides were incubated with the secondary antibodies Alexa 488 (Invitrogen A48262) and Alexa 568 (Invitrogen, A-11077) for MECA32 and CD31, respectively.

For the analysis of the PAS staining, 25 glomeruli per section were annotated in CaseViewer and the perimeter and the area of the glomeruli written down. To calculate mesangial area, annotations of the glomeruli were analysed with ImageJ (Fiji). The percentage of fibrotic tissue and collagen I was also calculated in CaseViewer.

2.9 | qPCR Analysis

RNA was isolated by using RNeasy Mini Kit (Qiagen, 74 106) according to manufacturer's instructions. cDNA was then produced from the RNA using M-MLV Reverse Transcriptase Kit (M1701, Promega), while qRT-PCR was performed with SYBR Select Master Mix (4 472 908, Applied Biosystems). Forward and reverse primers of the following genes have been used to perform qRT-PCR analysis:

Gene name	Forward sequence 5′ → 3′	Reverse sequence 3′ → 5′
Claudin 5	CTTCCTGGACCACAACAT CGTG	CACCGTCGGATCATAGAA CTCG
Col1	TGACTGGAAGAGCGGAGAGT	GTTCGGGCTGATGTACCAGT
Col3	TGGTCCTCAGGGTGTAAAGG	GTCCAGCATCACCTTTTGGT
Col4	CTGGAGAAAAGGGCCAGAT	TCCTTAACTTGTGCCTGTCCA
Drp1	GCGCTGATCCCGCGTCAT	CCGCACCCACTGTGTTGA
Fis1	GCCCCTGCTACTGGACCAT	CCCTGAAAGCCTCACACTAAGG
Gapdh	ACTCCCACTCTTCCACCTTC	CACCACCCTGTTGCTGTAG
Il1b	GCTACCTGTGTCTTTCCC	TCGTTGCTTGGTTCTCCTTG
Mcp1	TGATCCCAATGAGTAGGCTGGAG	ATGTCTGGACCCATTCCTTCTTG
Nos3	ATAGCCCGCATAGCGTATCAG	TCAGCCATCACAGTGTTCCC
Occludin	GAAAGTCCACCTCCTTAC AGACC	CATAGCCTCTGTCCCAAG CAAG
Pcg1a	GGACAGTCTCCCCGTGGAT	TCCATCTGTCAGTGCATCAAATG
Tgfb	GCAACATGTGGAACTCTACCAGAA	GACGTCAAAAGACAGCCACTCA
Tlr4	CCTGATGACATTCCTTCTTCAAC	TTGTTTCAATTTCACACCTGGATAAA
Ve-cadherin	CACTGCTTTGGGAGCCTTC	CACTGCTTTGGGAGCCTTC

2.10 | Transmission Electron Microscopy (TEM)

Kidney tissues were fixed for 1.5 h with 1.5% glutaraldehyde and 1% PFA (Electron Microscopy Sciences, Hatfield, PA) in 0.1 M sodium-cacodylate buffered solution. Samples were then further processed as previously described [36] and analysed by using either a G^2 Spirit BioTWIN transmission electron microscope (FEI, Eindhoven, The Netherlands), equipped with a FEI 4k Eagle CCD camera or a FEI Tecnai G^2 12 TWIN electron microscope, equipped with a Gatan OneView camera (Gatan, Pleasanton, CA). Image mosaics containing hundreds of images each were recorded with at 6500× or 6800× magnification, corresponding to a 3.4 and 3.25 nm pixel size at the specimen level. Images were collected and stitched together using automated data acquisition and stitching software [37].

2.11 | Metabolite Extraction of Plasma Samples for LC–MS/MS Analysis

To 50 μL plasma, 1 mL acetonitrile was added. Samples were vortexed vigorously and kept at −20°C for 45 min to allow proteins precipitation. After centrifugation at 18000 × g at 4°C for 15 min supernatants were collected and fully dried in a SpeedVac (Eppendorf, model 5301) before being stored at −80°C until further analysis. On the day of analysis, samples were reconstituted in 100 μL of a 1% methanol in water solution, vortexed and sonicated for 5 min. After centrifugation at 18000 × g at 4°C for 5 min, supernatants were transferred into micro-vial inserts and placed in the autosampler. A quality control (QC) sample was made by pooling an aliquot from all samples periodically measured across the analysis batch.

2.12 | Untargeted Metabolomics Analysis by LC–MS/MS

Plasma metabolites were measured using a liquid chromatography tandem mass spectrometry (LC–MS/MS) system, in combination with an in-house metabolite library [38], following previously described protocols [39]. Briefly, 10 μL of plasma extracts were analysed using a Shimadzu Nexera X2 (Shimadzu, the Netherlands) liquid chromatography system coupled to a Sciex TripleTOF mass spectrometer (MS). The mobile phases, that is, water (eluent A) and methanol (eluent B), both containing 0.1% formic acid, were delivered at 0.4 mL/min with the following gradient: 0% B at 0 min, 0% B at 1.5 min, 97% B at 9.9 min, 97% B at 12.9 min, 0% B at 13.0 min and 0% B at 13.8 min. The column used was a Synergi Hydro-RP, 2.5 μm, 100 × 2 mm with a Phenomenex SecurityGuard Ultra C8, 2.7 μm, 5 × 2.1 mm guard column cartridge, both were kept at 40°C. The MS was a Sciex TripleTOF 6600 (AB Sciex Netherlands B.V., The Netherlands) operated in positive and negative electrospray ionisation (ESI) mode, with the following conditions: ion source gas 1 50 psi, ion source gas 2 50 psi, curtain gas 30 psi, temperature 500°C, acquisition range m/z 75–650, ion spray voltage 5500 V (ESI+) and −4500 V (ESI−) and declustering potential 80 V (ESI+) and −80 V (ESI−). An information dependent acquisition (IDA) method was used to identify the observed metabolites, with the following conditions: collision energy ±10, acquisition time 80 ms and for MS/MS analysis: collision energy ±30, collision energy spread 15, ion release delay 30, ion release width 15 and acquisition time 40 ms. The IDA switching criteria was to exclude isotopes within 4 Da for a maximum of 18 candidate ions per cycle. MS-DIAL (v5.1), was used to align the data and annotate the different metabolites matching accurate mass, retention time and, in most cases, the MS/MS fragmentation pattern against the authentic chemical standards (in-house metabolite database). Metabolites with peak areas below 30% RSD across QC samples and sample-to-blank ratio above 5 for at least 80% of the samples within the experimental groups were considered for further data analysis. Data was further normalised using Probabilistic Quotient Normalisation (PQN).

2.13 | Microbiome Analysis and Sequencing

Faecal samples from week 0 and week 4, as well as the caecum samples from endpoint were used for 16S sequencing ($n = 10$ per group for each timepoint). Thirty nanograms of qualified DNA template and the 16S rRNA fusion primers (338F forward primer: ACTCCTACGGGAGGCAGCAG; 806R reverse primer: GGACTACHVGGGTWTCTAAT) were added for PCR. All PCR products were purified by Agencourt AMPure XP beads (Beckman Coulter Inc., Brea, California, USA), dissolved in Elution Buffer and eventually labelled to finish library construction. Library size and concentration were detected by Agilent 2100 Bioanalyzer. Qualified libraries were sequenced on the DNBSEQ-G400 platform according to their insert size. The QIIME 2 2023.9.1 tool was used to process the data and statistical analyses were performed in R version 4.1.1. Briefly, the raw sequence data were denoised and quality filtered with the DADA2 plugin (via 'denoise-paired') [40]. The obtained representative sequences were classified with the feature-classifier plugin (via 'classify-sklearn') [41] using the pre-trained Silva 138.1 animal-distal-gut taxonomy classifier. For statistical analyses, Phyloseq package (version 1.36.0) [42] was used to integrate the counts matrix, taxonomy and metadata. To determine α-diversity (presented as Shannon index), the package's function "estimate richness" was used and a one-way ANOVA was performed to compare the groups. Bray–Curtis dissimilarity index was used to calculate the β-diversity, with PERMANOVA testing to quantify the differences between the groups. For the identification of taxa changed between the groups, SIAMCAT [43] (version 1.12, abundance filtering = 0.01) were used with a false discovery rate correction = 0.05. Default parameters were used across analyses unless otherwise specified. Data was visualised with Ggplot2 (version 3.5.1). For the correlation analysis, microViz package (version 0.11.0) [44] was used to correlate the features of interest (GFR) with top 20 most abundant genera. Significant correlation with R higher or equal to 0.5 are shown.

2.14 | Statistical Analysis

Differences between groups have been assessed with two-way mixed model, with parametric or non-parametric unpaired *t*-test, or with correlation analysis, where appropriate. *p*-values of < 0.05 have been considered statistically significant, with $^*p < 0.05$, $^{**}p < 0.01$. The results are shown as mean ± SD.

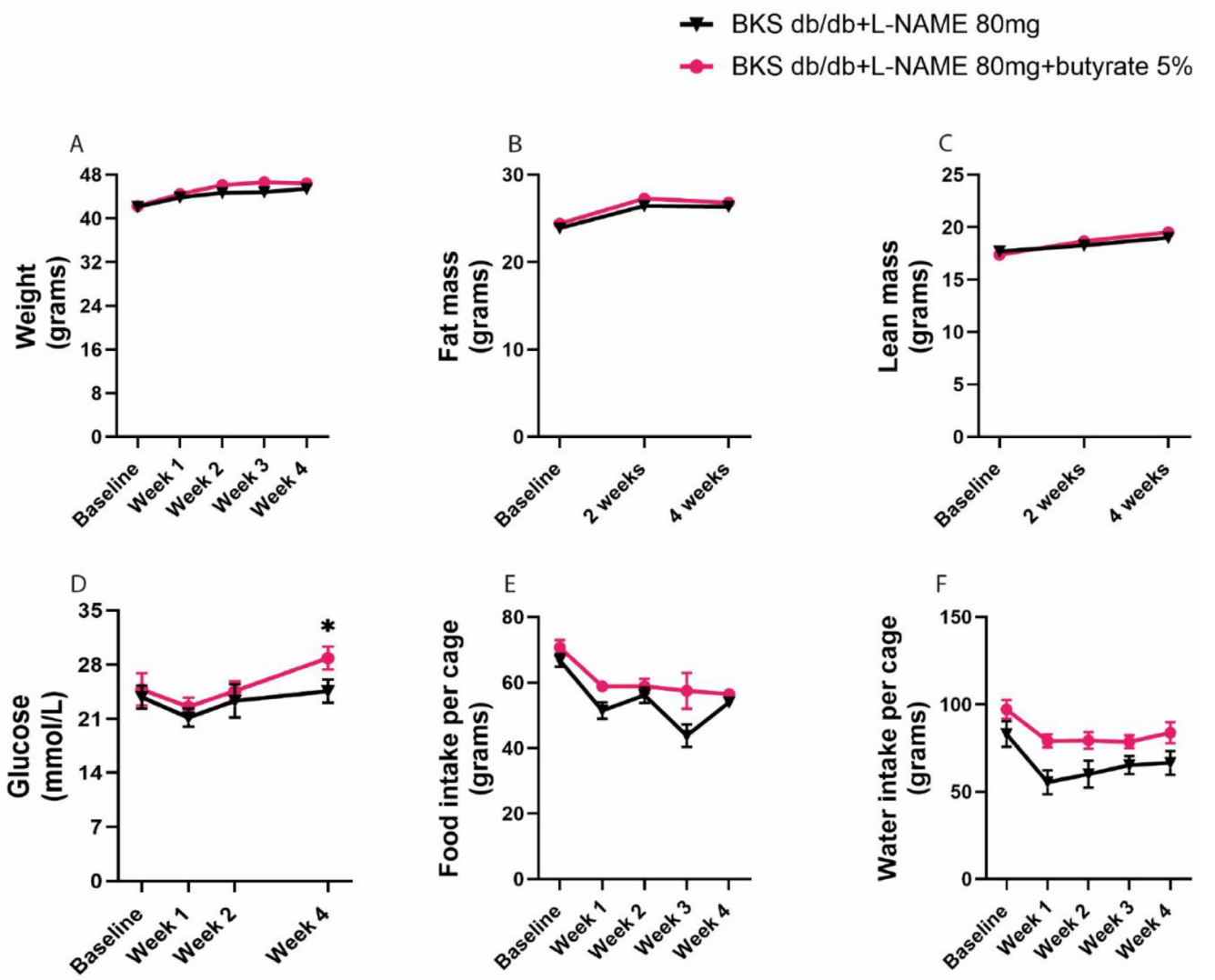

FIGURE 1 | Oral butyrate supplementation to mice treated with 80 mg of L-NAME does not affect fat mass, lean mass, food and water intake and increases blood glucose at week 4. Mice with DKD were fed a diet without or with 5% (w/w) butyrate treated and body weight (A), fat mass (B) lean mass (C), blood glucose (D), food intake (E) and water intake (F) were measured up to 4 weeks of treatment. *$p < 0.05$.

3 | Results

3.1 | Butyrate Administration Does Not Affect Body Weight or Food and Water Intake in DKD Mice

Oral supplementation with butyrate did not influence total weight gain (Figure 1A), nor the gain of fat mass (Figure 1B) or lean mass (Figure 1C) during the course of the experiment. Butyrate supplementation slightly increased blood glucose levels after 4 weeks (+14.8%; $p < 0.05$) (Figure 1D), without affecting food intake (Figure 1E) or water intake (Figure 1F).

3.2 | Oral Butyrate Administration Decreases Body Water Without Affecting Albuminuria and GFR

Oral butyrate supplementation did not affect mean arterial blood pressure (Figure 2A), nor the heart rate of the mice (Figure 2B) after 3 weeks of intervention compared to control mice. After 4 weeks of intervention, oral butyrate decreased body water content (−4.6; $p < 0.05$) (Figure 2C). Butyrate did not affect albuminuria, nor at 3 or at 4 weeks (Figure 2D–F), or GFR after 3 weeks (Figure 2G,H).

3.3 | Oral Butyrate Supplementation Results in Smaller Glomeruli and Less Fibrosis in the Kidney Medulla

PAS staining of kidney biopsies (Figure 3A,B) revealed that oral butyrate supplementation did not influence Bowman capsule area (Figure 3C), but it did reduce glomerular tuft area (−6.3%; $p < 0.05$; Figure 3D) and glomerular mesangial area (−4.9%; $p < 0.01$; Figure 3E). Sirius red staining of the same biopsies (Figure 3F,G) showed that oral butyrate did not affect fibrosis in kidney cortex (Figure 3H), while it reduced fibrotic tissue in the kidney medulla (−17.9%; $p < 0.05$; Figure 3I). Collagen I staining (Figure 3J,K) on the other hand showed that oral butyrate did not affect Collagen I deposition in either kidney cortex (Figure 3L) or kidney medulla (Figure 3M).

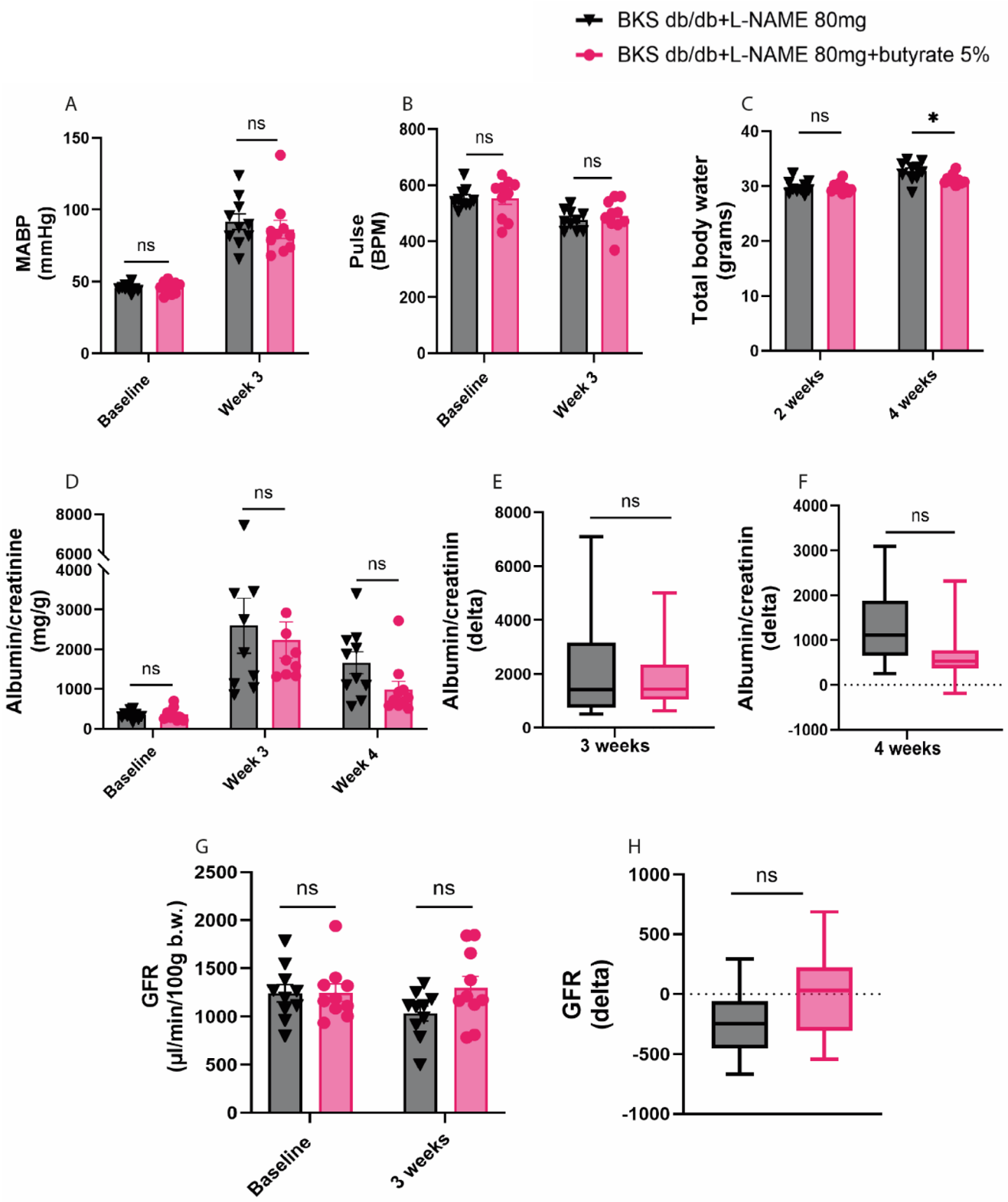

FIGURE 2 | Oral butyrate supplementation to mice treated with 80 mg of L-NAME does not affect mean arterial blood pressure, pulse, albumin/creatinine ratio and glomerular filtration rate, while decreasing the total body water content at week 4. Mean arterial blood pressure, MABP, (A) and pulse (B) of mice from both groups were measured at baseline and after 3 weeks the beginning of treatments, while total body water (C) and albumin-to-creatinine ratio (D) were measured for up to 4 weeks. For albumin-to-creatinine ratio, differences from baseline at 3 weeks (E) and 4 weeks (F) were also considered. Glomerular filtration rate, GFR, was also measured at baseline and 3 weeks after the beginning of the treatments (G), as well as the difference in GFR at baseline and 3 weeks (H). *$p < 0.05$.

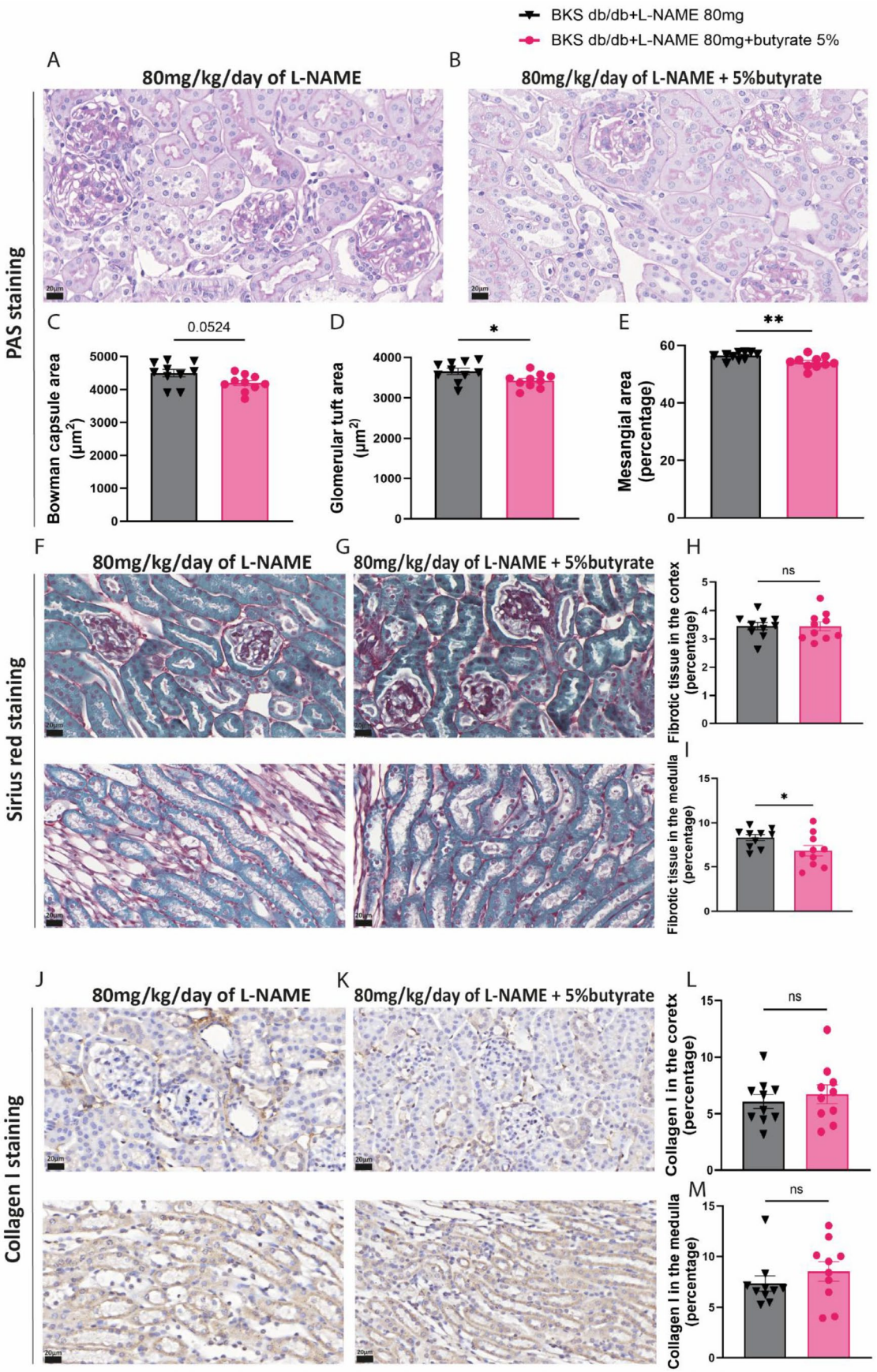

FIGURE 3 | Legend on next page.

FIGURE 3 | Oral butyrate supplementation to mice treated with 80 mg of L-NAME reduces glomerular tuft area and mesangial expansion, as well as fibrotic tissue deposition in renal medulla. PAS staining of kidney sections of mice from both groups (A, B) was performed and used to measure Bowman capsule area (C), glomerular tuft area (D), and glomerular mesangial area (E). Sirius red staining was also performed on the same kidney slices (F, G) to quantify cortical fibrosis (H) and medullar fibrosis (I), as well as Collagen I staining (J, K) to quantify Collagen I deposition in cortex (L) and medulla (M). $*p < 0.05$, $**p < 0.01$.

3.4 | Oral Butyrate Supplementation Affects Gut Microbiome Composition and Increases the Prevalence of *Akkermansiaceae* in Both Faeces and Caecum Content

The Shannon index calculation did not show changes in the gut microbiome alpha diversity after 4 weeks of butyrate intervention (Figure 4A). The Bray-Curtis index (beta-diversity) indicates microbial shift in the intervention group after 4 weeks of treatment, while control group microbial composition stayed the same (Figure 4B). When looking at the intestinal microbiome composition more specifically, both phyla (Figure 4C) and families (Figure 4D) of the bacteria changed over time in the intervention group. In the latter, the phylum of *Verrucomicrobiota* emerged at 4 weeks, while the control group showed a more conserved gut microbiome composition, where *Verrucomicrobiota* was not detected. When looking at families, in the intervention group *Akkermansiaceae*, the only family of the *Verrucomicrobiota* phylum, *Clostridia_UCG-014* and *Erysipelotrichaceae* were increased after 4 weeks of treatment, at the expense of *Lactobacillaceae* and *Lachnospiraceae*. On the other hand, the control group retained the same family diversity when compared to baseline. Moreover, the increase in *Akkermansiaceae* in the intervention group positively correlated with GFR (Figure 4E), on the contrary *Lactobacillaceae* abundancy negatively correlated with GFR (Figure 4F).

3.5 | Untargeted Metabolomics Analysis of Plasma Samples Revealed a Strong Positive Correlation Between Indole-3-Acetaldhyde, Indole-3-Methyl Acetate and *Akkermansiaceae*

Untargeted metabolomics analysis of plasma samples was able to identify the most abundant circulating metabolites, which were then correlated with the 20 genera that differed the most between the two groups (Figure 5). Amongst all the identified metabolites (Table S1), indole-3-acetaldehyde showed the strongest positive correlation to *Akkermansiaceae*.

4 | Discussion

In this study, we investigated the effects of oral butyrate administration in a mouse model of DKD. Our results showed that a butyrate-enriched diet does not directly affect kidney function within the experimental period. However, oral butyrate supplementation significantly altered glomerular morphology. Although these changes were not evident by electron microscopy (Figure S1), PAS staining analysis showed reduced glomerular size and mesangial area in the butyrate-treated group compared with controls. In addition, butyrate supplementation induced a shift in gut microbiome composition, marked by an increase in the *Akkermansiaceae* family, which was virtually absent in faecal and caecum samples from both groups prior to the intervention and remained scarce in the control group. Moreover, this increase in *Akkermansiaceae* abundance positively correlated with plasma levels of indole-3-methyl acetate and indole-3 acetaldehyde, metabolites traditionally associated with beneficial effects on human health [45].

The effect of oral butyrate administration especially in combination with high-fat diet had been widely studied, with previous research highlighting that in mice oral butyrate counteracts high-fat diet-induced weight gain [32, 46–48] and hyperglycemia [49–51]. These beneficial effects of butyrate-enriched diets rely on different factors, including decreased appetite and increased sense of satiety [28], enhanced fatty acid oxidation [52] and improved insulin sensitivity [53, 54]. Interestingly, when evaluating weight and glycemia, we not only failed to observe a reduction in these parameters following butyrate administration, but also found that, by week 4, the intervention group had higher blood glucose levels compared to the control group. Although these findings contrasted with much of the existing literature, our previous work [31] demonstrated that BKS db/db mice treated with L-NAME alone exhibited significantly less weight gain than untreated BKS db/db mice, likely due to slower digestion resulting from reduced vascular relaxation [55, 56]. Therefore, increased food intake and blood glucose might be the consequence of butyrate counterbalancing the reduction of NO [20, 57] or more broadly the general sense of discomfort induced by L-NAME.

When looking more specifically at the effect of butyrate on kidneys, renal function, measured by albumin-to-creatinine ratio and glomerular filtration rate (GFR), was not improved by butyrate administration when compared to the control group. At a tissue level, butyrate did not affect the expression of endothelial markers (Figures S2 and S3). Despite this, kidney biopsies from the control group showed enlarged glomeruli, mesangial expansion and medullary fibrosis. These observations suggest that alterations in the expression of the endothelial markers MECA32 and CD31 are not required to initiate kidney injury and that fibrosis and renal damage may develop before substantial vascular damage becomes evident. Supporting the hypothesis that renal injury is already occurring, mice in the control group exhibited a significantly higher body water content than those in the butyrate-treated group at 4 weeks. This increase in total body water may reflect fluid retention, an early manifestation of impaired kidney function [43].

Therefore, histological analysis suggested a protective effect of butyrate against kidney damage, with the selected time frame being excessively stringent to pick up changes in kidney function in vivo. This protective effect might be mediated both directly by butyrate and indirectly through modulation of the gut microbiome composition, which exhibited a significant shift from baseline, particularly in the intervention group.

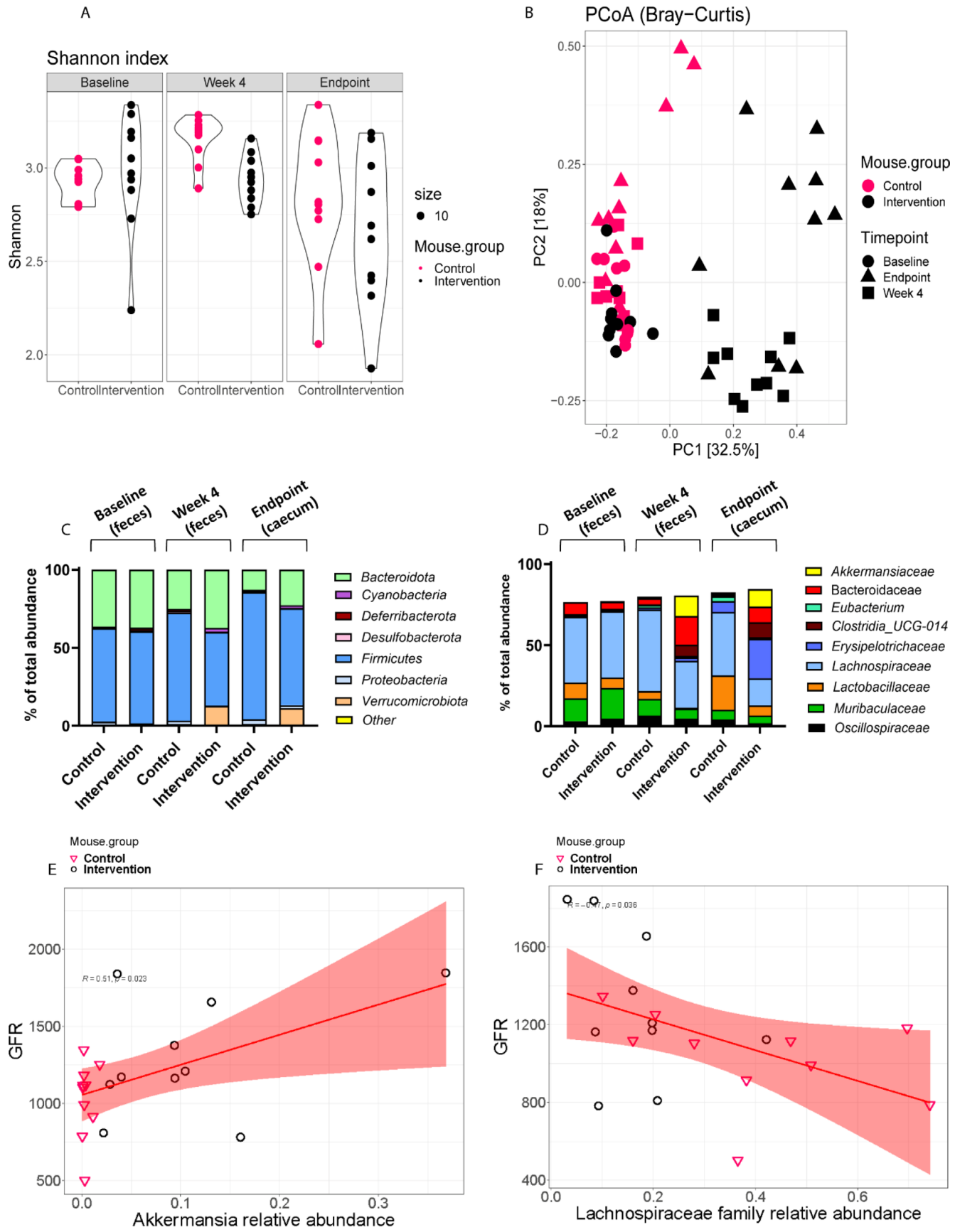

FIGURE 4 | Legend on next page.

FIGURE 4 | Oral butyrate supplementation to mice treated with 80 mg of L-NAME shifts the composition of the gut microbiome and increases *Akkermansiaceae*, which positively correlates with glomerular filtration rate and six plasma metabolites. Plots of Shannon index (A) and Bray-Curtis index (B) represent the diversity between the gut microbiome of the mice treated with 80 mg of L-NAME without and with 5% butyrate when comparing its composition at baseline and after 4 weeks of treatment, respectively. The composition of the gut microbiome in terms of families (C) and phyla (D) was analysed at baseline and at endpoint, while correlation between glomerular filtration rate (GFR) and *Akkermansiaceae* (E) and correlation between GFR and *Lachnospiraceae* (F) was analysed only for caecum samples.

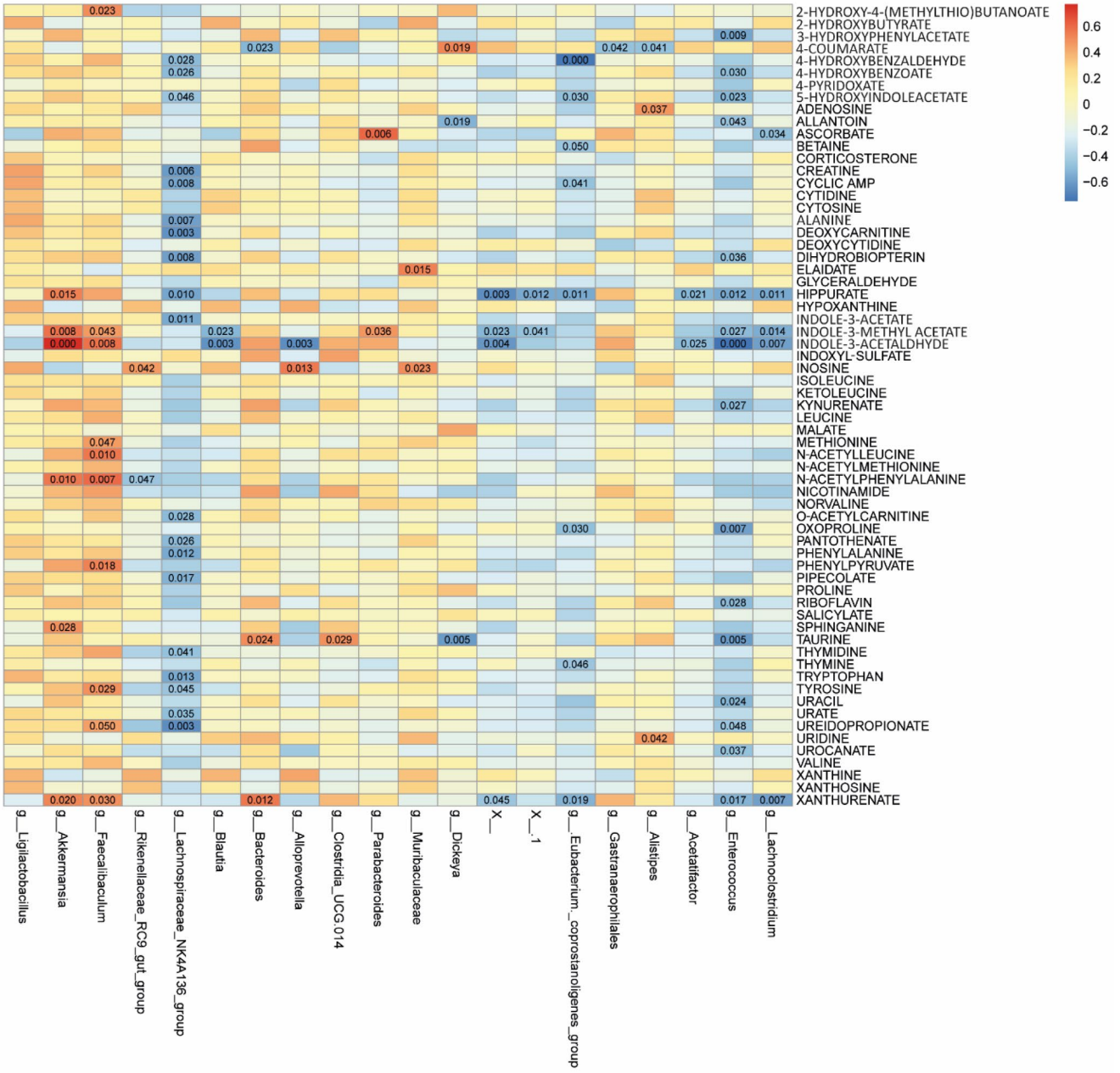

FIGURE 5 | Gut microbiota composition and cecum bile acids correlation is represented with a heatmap, where Spearman's rho non-parametric correlation was adopted.

Specifically, the genus of *Akkermansiaceae* distinctively emerged upon intervention with butyrate. *Akkermansiaceae* produce SCFAs by metabolising mucin [58] and its production in the intestine is increased by butyrate [59]. Previous studies have shown that this short-chain fatty acid can enhance mucin production in intestinal epithelial cells [60, 61], thereby increasing the availability of substrates utilised by Akkermansiaceae. Recent evidence suggests that butyrate modulates intestinal mucin production through activation of mitogen-activated protein kinase (MAPK) signalling pathways, which may stimulate mucin secretion and support Akkermansiaceae proliferation [62]. *Akkermansiaceae* are

generally associated with positive effects, including improved intestinal barrier [63] and host metabolism [64], possibly because of their correlation with tryptophan. Interestingly, indole-3-methyl acetate and indole-3-acetaldehyde (IAA), two products of tryptophan metabolism, showed the strongest positive correlation with *Akkermansiaceae* amongst all the detected metabolites, implying that the higher the bacteria from *Akkermansiaceae* the higher levels of these two metabolites in plasma. Especially IAA has been linked with positive effects on inflammation, immune system, obesity and blood sugar level [65], which ultimately might positively reflect on DKD. Moreover, the positive correlation between *Akkermansiaceae* abundance and GFR suggested that butyrate might support kidney function by promoting the outgrowth of these bacteria in the gut and enhancing the production of their associated metabolites that act on the kidney.

These metabolites may contribute to the modulation of inflammatory and oxidative stress pathways through mechanisms involving gut-kidney axis signalling and aryl hydrocarbon receptor (AhR)-related pathways. Activation of AhR signalling by tryptophan-derived indole metabolites has been associated with the regulation of immune responses, maintenance of epithelial barrier integrity and suppression of pro-inflammatory cytokine production [66]. In addition, these pathways may influence oxidative stress responses and cellular metabolic homeostasis, including mitochondrial function, which is often impaired during DKD progression [67]. By reducing systemic inflammation and limiting the translocation of pro-inflammatory bacterial products from the gut into the circulation, these metabolites may indirectly alleviate renal injury and fibrosis [68]. This would be in line with our observations, as reduction of medullary fibrotic tissue has been observed upon treatment with butyrate. However, qPCR analysis of inflammatory and immune-related markers, including Il1β, Tlr4 and Mcp1 (Figure S3), revealed no significant differences between the two experimental groups. These findings suggest that the beneficial effects of butyrate observed within the selected time frame are likely to be mediated by other mechanisms rather than a direct prominent effect on acute renal inflammation.

Although causality cannot be established in the present study, these findings support the hypothesis that microbiome-derived tryptophan metabolites may represent an important mechanistic link between butyrate supplementation and renal protection.

4.1 | Study Limitations

One of the main limitations of this study is the selected time frame. While histological and gut microbiome analyses suggested potential benefits of butyrate, these effects were not consistently reflected in most in vivo parameters. Renal function showed a promising trend, but it was not statistically significant and therefore remained inconclusive. For this reason, future studies involving longer periods of butyrate exposure may help to better define the timeframe required for butyrate to exert measurable effects on kidney function. Since animals tend to develop undesired and sometimes severe side effects upon exposure to L-NAME between 4 and 6 weeks, longer butyrate exposure should be carried out with preventive purposes, before L-NAME administration One technical limitation of the study is represented by the fact that the animals from the 2 groups have been euthanised on the same day but at different times, potentially influencing some of the physiological parameters measured at end point, for instance blood glucose measurements. Most of the animals from the butyrate group remained awake for longer due to the experimental schedule before the glucose was measured and therefore, they could have access to food for longer. This might have influenced the value of glycemia measured at week 4. Lastly, a potential translational limitation is the difference between the gut microbiomes of laboratory mice and humans. Although C57BL/6 mice exhibit a similar prevalence of SCFA-producing bacteria compared to humans the overall gut microbiome composition between the two species is substantially different [69], with possible even greater discrepancies in BKS db/db mice. When considering human application, it would be valuable to first perform additional preclinical studies in healthy mice to establish a potential threshold for butyrate toxicity. Administering progressively increasing doses of butyrate to healthy animals could help determine the maximum tolerated dose and provide guidance on exposure levels that should not be exceeded when translating these findings to humans.

5 | Conclusion

Oral treatment with butyrate influences renal structure and gut microbiome composition, without affecting body weight, food intake, albuminuria and GFR. Specifically, oral administration of butyrate greatly boosted the family of *Akkermansiaceae*, which has been emerging as very promising prebiotics for human health and might therefore be responsible for the improved histological features observed in animals treated with butyrate. Further studies are required to establish a causal relationship between oral butyrate administration, the enrichment of Akkermansiaceae and the potential beneficial effects observed on kidneys. For instance, single metabolite and/or single bacterial strain experiments would greatly help to clarify whether butyrate is ultimately responsible for boosting Akkermansiaceae and whether the latter produce metabolites capable of influencing kidney function. In vitro experiments exposing renal cells to metabolites of interest, including indole-3-methyl acetate and indole-3-acetaldehyde, may help elucidate the molecular pathways through which these compounds influence renal function.

Another mechanism that has not yet been explored but may also contribute to the reno-protective effects of butyrate in our model is its ability to counteract the L-NAME-induced increase in intestinal permeability. L-NAME has been shown to exacerbate intestinal hyperpermeability [70, 71], an effect that butyrate has been reported to attenuate in patients with irritable bowel syndrome (IBS) [72]. Since individuals with diabetes frequently exhibit increased intestinal permeability, which has been associated with the development and progression of diabetic kidney disease [73], butyrate may also exert beneficial effects on DKD by preserving intestinal barrier integrity.

If further research confirms that butyrate also benefits kidney function, a diet aimed at boosting butyrate metabolism could become a valuable strategy for strengthening the gut microbiome

and helping to prevent or slow the progression of diabetic kidney disease.

Acknowledgements

We would like to thank Dr. Sabine Neudecker and Dr. Daniel Schock-Kusch from MediBeacon for their support and help with GFR measurements and analysis.

Funding

This work was supported by the Rembrandt Institute of Cardiovascular Science (RICS) (80640).

Conflicts of Interest

M.N. Nicese, A. Koudijs, S. Kooijman, P.C.N. Rensen, R. Bijkerk, B.M. van den Berg and J.I. Rotmans contributed to the study design. M.N. Nicese, A. Koudijs, A.C.M. Pronk and B.M. van den Berg contributed to conducting experiments and collecting data. M.N. Nicese, A. Koudijs, L. Reshma, R.J.E. Derks, E. Sánchez-López, M. Giera, A. Kovynev and B.M. van den Berg helped with performing the analysis of the data. M.N. Nicese, P.C.N. Rensen, R. Bijkerk, B.M. van den Berg and J.I. Rotmans contributed to writing the manuscript, which has been subsequently revised and approved by all the co-authors.

Data Availability Statement

The data that support the findings of this study are available from the corresponding author upon reasonable request.

Peer Review

The peer review history for this article is available at https://www.webofscience.com/api/gateway/wos/peer-review/10.1111/dom.71245.

References

1. S. B. Ghaderian, F. Hayati, S. Shayanpour, and S. S. Beladi Mousavi, "Diabetes and End-Stage Renal Disease; a Review Article on New Concepts," *Journal of Renal Injury Prevention* 4, no. 2 (2015): 28–33.

2. E. K. Hoogeveen, "The Epidemiology of Diabetic Kidney Disease," *Kidney and Dialysis* 2, no. 3 (2022): 433–442.

3. V. Natesan and S. J. Kim, "Diabetic Nephropathy: A Review of Risk Factors, Progression, Mechanism, and Dietary Management," *Biomolecules & Therapeutics* 29, no. 4 (2021): 365–372.

4. N. Samsu, "Diabetic Nephropathy: Challenges in Pathogenesis, Diagnosis, and Treatment," *BioMed Research International* 2021 (2021): 1497449.

5. P. N. Van Buren and R. Toto, "Hypertension in Diabetic Nephropathy: Epidemiology, Mechanisms, and Management," *Advances in Chronic Kidney Disease* 18, no. 1 (2011): 28–41.

6. Z. Cao and M. E. Cooper, "Pathogenesis of Diabetic Nephropathy," *Journal of Diabetes Investigation* 2, no. 4 (2011): 243–247.

7. X. He, J. Sun, C. Liu, et al., "Compositional Alterations of Gut Microbiota in Patients With Diabetic Kidney Disease and Type 2 Diabetes Mellitus," *Diabetes, Metabolic Syndrome and Obesity: Targets and Therapy* 15 (2022): 755–765.

8. J. R. Lin, Z. T. Wang, J. J. Sun, et al., "Gut Microbiota and Diabetic Kidney Diseases: Pathogenesis and Therapeutic Perspectives," *World Journal of Diabetes* 13, no. 4 (2022): 308–318.

9. Q. Zhang, H. Sheng, X. Hu, et al., "The Role of Gut Microbiota and Microbiota-Related Serum Metabolites in the Progression of Diabetic Kidney Disease," *Frontiers in Pharmacology* 12 (2021): 757508.

10. Y. Wang, J. Zhao, Y. Qin, et al., "The Specific Alteration of Gut Microbiota in Diabetic Kidney Diseases-A Systematic Review and Meta-Analysis," *Frontiers in Immunology* 13 (2022): 908219.

11. A. Zaky, S. J. Glastras, M. Y. W. Wong, C. A. Pollock, and S. Saad, "The Role of the Gut Microbiome in Diabetes and Obesity-Related Kidney Disease," *International Journal of Molecular Sciences* 22, no. 17 (2021): 9641.

12. A. Sabatino, G. Regolisti, C. Cosola, L. Gesualdo, and E. Fiaccadori, "Intestinal Microbiota in Type 2 Diabetes and Chronic Kidney Disease," *Current Diabetes Reports* 17, no. 3 (2017): 16.

13. E. Rinninella, P. Raoul, M. Cintoni, et al., "What Is the Healthy Gut Microbiota Composition? A Changing Ecosystem Across Age, Environment, Diet, and Diseases," *Microorganisms* 7, no. 1 (2019): 14.

14. P. Tao, J. Ji, Q. Wang, M. Cui, M. Cao, and Y. Xu, "The Role and Mechanism of Gut Microbiota-Derived Short-Chain Fatty in the Prevention and Treatment of Diabetic Kidney Disease," *Frontiers in Immunology* 13 (2022): 1080456.

15. R. G. Xiong, D. D. Zhou, S. X. Wu, et al., "Health Benefits and Side Effects of Short-Chain Fatty Acids," *Food* 11, no. 18 (2022): 2863.

16. Q. Yang, J. Ouyang, F. Sun, and J. Yang, "Short-Chain Fatty Acids: A Soldier Fighting Against Inflammation and Protecting From Tumorigenesis in People With Diabetes," *Frontiers in Immunology* 11 (2020): 590685.

17. D. Parada Venegas, M. K. de la Fuente, G. Landskron, et al., "Short Chain Fatty Acids (SCFAs)-Mediated Gut Epithelial and Immune Regulation and Its Relevance for Inflammatory Bowel Diseases," *Frontiers in Immunology* 10 (2019): 277.

18. G. Magliocca, P. Mone, B. R. di Iorio, A. Heidland, and S. Marzocco, "Short-Chain Fatty Acids in Chronic Kidney Disease: Focus on Inflammation and Oxidative Stress Regulation," *International Journal of Molecular Sciences* 23, no. 10 (2022): 5354.

19. M. Mazhar, Y. Zhu, and L. Qin, "The Interplay of Dietary Fibers and Intestinal Microbiota Affects Type 2 Diabetes by Generating Short-Chain Fatty Acids," *Food* 12, no. 5 (2023): 1023.

20. P. Amiri, S. A. Hosseini, S. Ghaffari, et al., "Role of Butyrate, a Gut Microbiota Derived Metabolite, in Cardiovascular Diseases: A Comprehensive Narrative Review," *Frontiers in Pharmacology* 12 (2021): 837509.

21. K. Hodgkinson, F. El Abbar, P. Dobranowski, et al., "Butyrate's Role in Human Health and the Current Progress Towards Its Clinical Application to Treat Gastrointestinal Disease," *Clinical Nutrition* 42, no. 2 (2023): 61–75.

22. Y. J. Li, X. Chen, T. K. Kwan, et al., "Dietary Fiber Protects Against Diabetic Nephropathy Through Short-Chain Fatty Acid-Mediated Activation of G Protein-Coupled Receptors GPR43 and GPR109A," *Journal of the American Society of Nephrology* 31, no. 6 (2020): 1267–1281.

23. M. N. Nicese, R. Bijkerk, A. J. van Zonneveld, B. M. van den Berg, and J. I. Rotmans, "Sodium Butyrate as Key Regulator of Mitochondrial Function and Barrier Integrity of Human Glomerular Endothelial Cells," *International Journal of Molecular Sciences* 24, no. 17 (2023): 13090.

24. S. Hu, R. Kuwabara, B. J. de Haan, A. M. Smink, and P. de Vos, "Acetate and Butyrate Improve Beta-Cell Metabolism and Mitochondrial Respiration Under Oxidative Stress," *International Journal of Molecular Sciences* 21, no. 4 (2020): 1542.

25. V. Karoor, D. Strassheim, T. Sullivan, et al., "The Short-Chain Fatty Acid Butyrate Attenuates Pulmonary Vascular Remodeling and Inflammation in Hypoxia-Induced Pulmonary Hypertension," *International Journal of Molecular Sciences* 22, no. 18 (2021): 9916.

26. Z. Gao, J. Yin, J. Zhang, et al., "Butyrate Improves Insulin Sensitivity and Increases Energy Expenditure in Mice," *Diabetes* 58, no. 7 (2009): 1509–1517.

27. M. Rios-Morales, M. A. Vieira-Lara, E. Homan, et al., "Butyrate Oxidation Attenuates the Butyrate-Induced Improvement of Insulin Sensitivity in Myotubes," *Biochimica et Biophysica Acta - Molecular Basis of Disease* 1868, no. 11 (2022): 166476.

28. Z. Li, C. X. Yi, S. Katiraei, et al., "Butyrate Reduces Appetite and Activates Brown Adipose Tissue via the Gut-Brain Neural Circuit," *Gut* 67, no. 7 (2018): 1269–1279.

29. T. J. Oh, W. J. Sul, H. N. Oh, et al., "Butyrate Attenuated Fat Gain Through Gut Microbiota Modulation in Db/Db Mice Following Dapagliflozin Treatment," *Scientific Reports* 9, no. 1 (2019): 20300.

30. G. Tang, Y. du, H. Guan, et al., "Butyrate Ameliorates Skeletal Muscle Atrophy in Diabetic Nephropathy by Enhancing Gut Barrier Function and FFA2-Mediated PI3K/Akt/mTOR Signals," *British Journal of Pharmacology* 179, no. 1 (2022): 159–178.

31. M. N. Nicese, A. Koudijs, R. Lalai, et al., "Oral L-NAME Supplementation Accelerates the Progression of Kidney Disease in Diabetic Mice," *Biochemical and Biophysical Research Communications* 790 (2025): 152859.

32. J. Yang, G. Li, S. Wang, et al., "Butyrate Prevents Obesity Accompanied by HDAC9-Mediated Browning of White Adipose Tissue," *Biomedicine* 13, no. 2 (2025): 260.

33. Z. Li, E. Zhou, C. Liu, et al., "Dietary Butyrate Ameliorates Metabolic Health Associated With Selective Proliferation of Gut Lachnospiraceae Bacterium 28-4," *JCI Insight* 8, no. 4 (2023): e166655.

34. H. V. Lin, A. Frassetto, E. J. Kowalik Jr, et al., "Butyrate and Propionate Protect Against Diet-Induced Obesity and Regulate Gut Hormones via Free Fatty Acid Receptor 3-Independent Mechanisms," *PLoS One* 7, no. 4 (2012): e35240.

35. L. Scarfe, D. Schock-Kusch, L. Ressel, et al., "Transdermal Measurement of Glomerular Filtration Rate in Mice," *Journal of Visualized Experiments* 140 (2018): e58520.

36. B. M. van den Berg, G. Wang, M. G. S. Boels, et al., "Glomerular Function and Structural Integrity Depend on Hyaluronan Synthesis by Glomerular Endothelium," *Journal of the American Society of Nephrology* 30, no. 10 (2019): 1886–1897.

37. F. G. Faas, M. C. Avramut, B. M. Berg, A. M. Mommaas, A. J. Koster, and R. B. Ravelli, "Virtual Nanoscopy: Generation of Ultra-Large High Resolution Electron Microscopy Maps," *Journal of Cell Biology* 198, no. 3 (2012): 457–469.

38. A. Ciurli, Y. Mohammed, C. Ammon, et al., "Spatially and Temporally Resolved Metabolome of the Human Oral Cavity," *iScience* 27, no. 2 (2024): 108884.

39. S. Singh, L. B. Giron, M. W. Shaikh, et al., "Distinct Intestinal Microbial Signatures Linked to Accelerated Systemic and Intestinal Biological Aging," *Microbiome* 12, no. 1 (2024): 31.

40. B. J. Callahan, P. J. McMurdie, M. J. Rosen, A. W. Han, A. J. A. Johnson, and S. P. Holmes, "DADA2: High-Resolution Sample Inference From Illumina Amplicon Data," *Nature Methods* 13, no. 7 (2016): 581–583.

41. N. A. Bokulich, B. D. Kaehler, J. R. Rideout, et al., "Optimizing Taxonomic Classification of Marker-Gene Amplicon Sequences With QIIME 2's q2-Feature-Classifier Plugin," *Microbiome* 6, no. 1 (2018): 90.

42. P. J. McMurdie and S. Holmes, "Phyloseq: An R Package for Reproducible Interactive Analysis and Graphics of Microbiome Census Data," *PLoS One* 8, no. 4 (2013): e61217.

43. J. Wirbel, K. Zych, M. Essex, et al., "Microbiome Meta-Analysis and Cross-Disease Comparison Enabled by the SIAMCAT Machine Learning Toolbox," *Genome Biology* 22, no. 1 (2021): 93.

44. D. Barnett, I. Arts, and J. Penders, "microViz: An R Package for Microbiome Data Visualization and Statistics," *Journal of Open Source Software* 6, no. 63 (2021): 3201.

45. X. Ye, H. Li, K. Anjum, et al., "Dual Role of Indoles Derived From Intestinal Microbiota on Human Health," *Frontiers in Immunology* 13 (2022): 903526.

46. V. A. Matheus, L. C. S. Monteiro, R. B. Oliveira, D. A. Maschio, and C. B. Collares-Buzato, "Butyrate Reduces High-Fat Diet-Induced Metabolic Alterations, Hepatic Steatosis and Pancreatic Beta Cell and Intestinal Barrier Dysfunctions in Prediabetic Mice," *Experimental Biology and Medicine (Maywood, N.J.)* 242, no. 12 (2017): 1214–1226.

47. T. M. Henagan, B. Stefanska, Z. Fang, et al., "Sodium Butyrate Epigenetically Modulates High-Fat Diet-Induced Skeletal Muscle Mitochondrial Adaptation, Obesity and Insulin Resistance Through Nucleosome Positioning," *British Journal of Pharmacology* 172, no. 11 (2015): 2782–2798.

48. W. Fang, H. Xue, X. Chen, K. Chen, and W. Ling, "Supplementation With Sodium Butyrate Modulates the Composition of the Gut Microbiota and Ameliorates High-Fat Diet-Induced Obesity in Mice," *Journal of Nutrition* 149, no. 5 (2019): 747–754.

49. A. Jiao, B. Yu, J. He, et al., "Sodium Acetate, Propionate, and Butyrate Reduce Fat Accumulation in Mice via Modulating Appetite and Relevant Genes," *Nutrition* 87–88 (2021): 111198.

50. W. Zhu, K. Peng, Y. Zhao, et al., "Sodium Butyrate Attenuated Diet-Induced Obesity, Insulin Resistance and Inflammation Partly by Promoting Fat Thermogenesis via Intro-Adipose Sympathetic Innervation," *Frontiers in Pharmacology* 13 (2022): 938760.

51. D. Zhou, Y. W. Chen, Z. H. Zhao, et al., "Sodium Butyrate Reduces High-Fat Diet-Induced Non-Alcoholic Steatohepatitis Through Upregulation of Hepatic GLP-1R Expression," *Experimental & Molecular Medicine* 50, no. 12 (2018): 1–12.

52. N. Hamari, E. E. Blaak, and E. E. Canfora, "The Impact of Butyrate on Glycemic Control in Animals and Humans: A Comprehensive Semi-Systemic Review," *Frontiers in Nutrition* 12 (2025): 1603490.

53. F. Gao, Y. W. Lv, J. Long, et al., "Butyrate Improves the Metabolic Disorder and Gut Microbiome Dysbiosis in Mice Induced by a High-Fat Diet," *Frontiers in Pharmacology* 10 (2019): 1040.

54. M. P. Mollica, G. Mattace Raso, G. Cavaliere, et al., "Butyrate Regulates Liver Mitochondrial Function, Efficiency, and Dynamics in Insulin-Resistant Obese Mice," *Diabetes* 66, no. 5 (2017): 1405–1418.

55. S. De Moudt, J. O. Hendrickx, C. Neutel, et al., "Aortic Stiffness in L-NAME Treated C57Bl/6 Mice Displays a Shift From Early Endothelial Dysfunction to Late-Term Vascular Smooth Muscle Cell Dysfunction," *Frontiers in Physiology* 13 (2022): 874015.

56. S.-C. G. Hui and T.-Y. Chan, "Mechanisms Mediating N G-Nitro-L-Arginine Methyl Ester-Induced Hypophagia in Mice," *European Journal of Pharmacology* 283 (1995): 141–150.

57. M. T. S. Dias, E. C. Aguilar, G. P. Campos, et al., "Butyrate Inhibits LPC-Induced Endothelial Dysfunction by Regulating nNOS-Produced NO and ROS Production," *Nitric Oxide* 138–139 (2023): 42–50.

58. H. Zhang, Y. Pan, Y. Jiang, et al., "*Akkermansia muciniphila* ONE Effectively Ameliorates Dextran Sulfate Sodium (DSS)-Induced Ulcerative Colitis in Mice," *Npj Science of Food* 8, no. 1 (2024): 97.

59. E. Gaudier, A. Jarry, H. M. Blottière, et al., "Butyrate Specifically Modulates MUC Gene Expression in Intestinal Epithelial Goblet Cells Deprived of Glucose," *American Journal of Physiology. Gastrointestinal and Liver Physiology* 287, no. 6 (2004): G1168–G1174.

60. S. M. Akira Shimotoyodome, T. Hase, I. Tokimitsu, and T. Sakata, "Short Chain Fatty Acids but Not Lactate or Succinate Stimulate Mucus Release in the Rat Colon," *Comparative Biochemistry and Physiology Part A, Molecular & Integrative Physiology* 125 (2000): 525–531.

61. L. E. M. Willemsen, M. A. Koetsier, S. J. H. van Deventer, and E. A. F. van Tol, "Short Chain Fatty Acids Stimulate Epithelial Mucin 2 Expression Through Differential Effects on Prostaglandin E1 and E2 Production by Intestinal Myofibroblasts," *Gut* 52 (2003): 1442–1447.

62. T. H. Jung, K. S. Han, J. H. Park, and H. J. Hwang, "Butyrate Modulates Mucin Secretion and Bacterial Adherence in LoVo Cells via MAPK Signaling," *PLoS One* 17, no. 7 (2022): e0269872.

63. W. Wu, W. Kaicen, X. Bian, et al., "*Akkermansia muciniphila* Alleviates High-Fat-Diet-Related Metabolic-Associated Fatty Liver Disease by Modulating Gut Microbiota and Bile Acids," *Microbial Biotechnology* 16, no. 10 (2023): 1924–1939.

64. M. I. D. Sanjiwani, I. P. H. Aryadi, and I. M. S. Semadi, "Review of Literature on Akkermansia Muciniphila and Its Possible Role in the Etiopathogenesis and Therapy of Type 2 Diabetes Mellitus," *Journal of the ASEAN Federation of Endocrine Societies* 37, no. 1 (2022): 69–74.

65. N. Shaheen, J. Miao, B. Xia, Y. Zhao, and J. Zhao, "Multifaceted Role of Microbiota-Derived Indole-3-Acetic Acid in Human Diseases and Its Potential Clinical Application," *FASEB Journal* 39, no. 11 (2025): e70574.

66. T. D. Hubbard, I. A. Murray, and G. H. Perdew, "Indole and Tryptophan Metabolism: Endogenous and Dietary Routes to Ah Receptor Activation," *Drug Metabolism and Disposition* 43, no. 10 (2015): 1522–1535.

67. C. S. Curran and J. B. Kopp, "Aryl Hydrocarbon Receptor Mechanisms Affecting Chronic Kidney Disease," *Frontiers in Pharmacology* 13 (2022): 782199.

68. J. R. Liu, H. Miao, D. Q. Deng, N. D. Vaziri, P. Li, and Y. Y. Zhao, "Gut Microbiota-Derived Tryptophan Metabolism Mediates Renal Fibrosis by Aryl Hydrocarbon Receptor Signaling Activation," *Cellular and Molecular Life Sciences* 78, no. 3 (2021): 909–922.

69. R. Nagpal, S. Wang, L. C. Solberg Woods, et al., "Comparative Microbiome Signatures and Short-Chain Fatty Acids in Mouse, Rat, Non-Human Primate, and Human Feces," *Frontiers in Microbiology* 9 (2018): 2897.

70. C. C. Chen, H. M. Chen, C. H. Chiu, L. N. Lin, and J. C. Chen, "Effect of NG-Nitro-L-Arginine Methyl Ester on Intestinal Permeability Following Intestinal Ischemia-Reperfusion Injury in a Rat Model," *Biology of the Neonate* 80 (2001): 60–63.

71. B. Li, X. He, S. S. Lei, et al., "Hypertensive Rats Treated Chronically With N(Omega)-Nitro-L-Arginine Methyl Ester (L-NAME) Induced Disorder of Hepatic Fatty Acid Metabolism and Intestinal Pathophysiology," *Frontiers in Pharmacology* 10 (2019): 1677.

72. M. W. Scharf, R. A. Forsgård, S. B. R. Prado, et al., "Acute Effects of Butyrate on Intestinal Permeability in Patients With Irritable Bowel Syndrome Assessed by a Novel Colonoscopy Research Model," *Gut Microbes* 17, no. 1 (2025): 2545414.

73. X. Zheng, X. Luo, Y. Zhang, et al., "Inflammation in Diabetic Kidney Disease Is Linked to Gut Dysbiosis and Metabolite Imbalance," *Journal of Diabetes* 17, no. 12 (2025): e70175.

Supporting Information

Additional supporting information can be found online in the Supporting Information section. **Figure S1:** Transmission electron microscopy (TEM) pictures of glomeruli from kidney biopsies of from BKS db/db mice +80 mg of L-NAME (A) and of BKS db/db mice +80 mg of L-NAME + butyrate (B), with detail of the glomerular basement membrane or GBM (C). The thickness of GBM has been calculated by multiplying its height by its base (D). **Figure S2:** MECA32 staining (A) with respective quantification (B) and CD31 staining (C) with respective quantification (D) of kidney biopsies of from BKS db/db mice +80 mg of L-NAME and of BKS db/db mice +80 mg of L-NAME + butyrate with respective quantifications. **Figure S3:** Quantitative PCR analysis of kidney tissue from BKS db/db mice +80 mg of L-NAME and of BKS db/db mice +80 mg of L-NAME + butyrate. The expression of the following genes has been analysed and quantified: Ve-cadherin (A), Claudin 5 (B), Occluding (C), Nos3 (D), IL1b (E), Tlr4 (F), Mcp1 (G), Drp1 (H), Pgc1a (I), FIS1 (J), Tgfb (K), Col I (L) Col III (M) and Col IV (N). **Table S1:** Averaged relative abundance of plasma identified metabolites normalised by Probabilistic Quotient Normalisation (PQN) for the two experimental groups ($n = 10$ per group).